ACS Photonics

Article

pubs.acs.org/journal/apchd5

Observation of Emission Enhancement Caused by Symmetric Carrier Depletion in III−V Nanomembrane Heterostructures

Lucas Atila Bernardes Marçal,[†] Barbara Luiza Teixeira Rosa,[†,‡] Gustavo A. M. Safar,[†] Raul O. Freitas,[§] Oliver G. Schmidt,[∥] Paulo Sergio Soares Guimarães,[†,‡] Christoph Deneke,[∥,⊥] and Angelo Malachias*[,†]

[†]Departamento de Física, Universidade Federal de Minas Gerais, Avenida Presidente Antônio Carlos 6627, 31270-901 Belo Horizonte, MG Brazil

[‡]DISSE-Instituto Nacional de Ciência e Tecnologia de Nanodispositivos Semicondutores, Rio de Janeiro, Brazil

[§]Laboratório Nacional de Luz Síncrotron (LNLS), Rua Giuseppe Máximo Scolfaro 10000, 13083-100 Campinas, SP, Brazil

[∥]IFW Dresden, Helmholtzstrasse 20, Dresden, Germany

[⊥]Laboratório Nacional de Nanotecnologia (LNNano/CNPEM), Rua Giuseppe Máximo Scolfaro 10000, 13083-100 Campinas, SP, Brazil

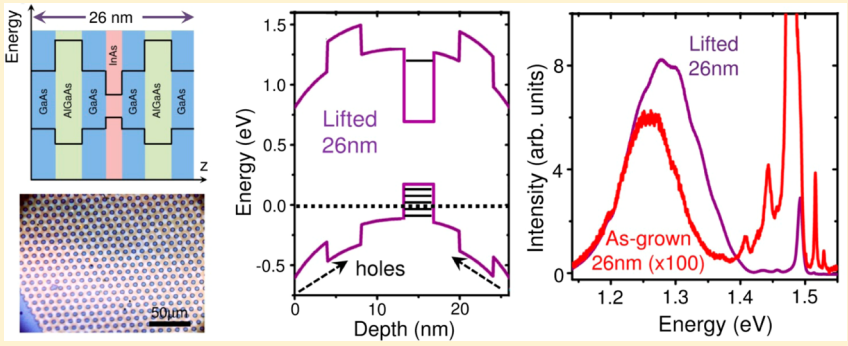

ABSTRACT: Semiconductor nanomembranes are promising systems for many applications, since the band structure of a given material can be tailored to achieve specific configurations, which are not feasible by conventional growth procedures on rigid substrates. Here we show that optically active III−V membranes containing InAs quantum dots exhibit a pronounced photoluminescence enhancement with respect to equivalent systems grown on top of flat substrates. The effect is explained by the formation of carrier depletion regions symmetrically located with respect to the optically active layer. This leads to the filling of excited states of the quantum dots and the overall spectra are enhanced at higher energies. Changes on the strain field that are expected to lead to a red-shift of the quantum dot emission play a reduced role in the final emission spectra in comparison with the depletion effects. These effects can be considered as another degree of freedom and a key ingredient for band engineering of extremely thin semiconductor membranes.

KEYWORDS: *semiconductor nanomembranes, heterostructures, X-ray diffraction, photoluminescence, carrier depletion*

In the past decade, the release and transfer of thin membranes have been extensively studied and gave rise to a promising field inside nanotechnology.[1−12] Works have been carried out both with inorganic as well as soft matter systems originally deposited as thin films on a variety of different rigid substrates. The demonstrated ability to transfer functional, nanometer thick, high-quality membranes (i.e., nanomembranes) has opened up a plethora of potential applications in flexible electronics and optoelectronics.[1,13−20] Among the most promising systems are thin semiconductor nanomembranes (NMs) containing optically active structures like quantum wells (QW) or self-assembled quantum dots (QD).[20−25] Recently, NMs transferred to piezo-electric host substrates have been successfully used to tune the embedded quantum emitters[21,22] by straining the transferred membrane.

In a first (naïve) expectation, the strain modifications of the transferred NM are the main relevant factor directly impacting on the optical properties of the embedded QD or QW, for example, when probed in photoluminescence (PL) experiments. In fact, a PL redshift of 11 meV on a strained QW inside a released and bound-back NM was already reported.[20] The strain relaxation of the NM causes a change on the band structure resulting in a red shift of the observed PL signal. Besides this work, a variety of released and rolled-up NMs have been investigated in the literature[23,26−29] and a clear connection of the strain state of the released layers with the optical signal has been reported.[23] The NM thickness in the works cited here ranged from 50 nm in rolled-up layers[23,30−32] to more than 200

Received: April 30, 2014
Published: August 14, 2014

nm in released two-dimensional membranes,[22,25,26] but ultrathin membranes of high technological interest have not been investigated.

Furthermore, wrinkled, bound-back, and rolled-up structures can only partially relax their strain. Therefore, investigating strain effects with structural techniques on a completely released film is necessary to fully understand such systems, for example, when used for tuning QD emissions.[21] Until now, the structural consequences in all investigated NMs point out to a red shift of the QD emission. Such behavior in PL spectra would denote lattice parameter changes that take place inside the QDs, but also the propagation of a modified strain field into the barrier layers.[23,33] In addition to a signal shift due to strain relaxation, an overall reduction of the PL intensity was observed for released and wrinkled NMs,[20] with a relative small enhancement due to interference effects reported for a wrinkled NM with respect to bound-back areas.

Normally, QDs or QWs grown in the vicinity of the surface have the drawback of producing a potential well located at the depletion regions. This undesirable effect, taking place in the proximity of any surface, is responsible for mitigating or removing carriers from confined states in the engineered wells due to the asymmetric overall potential bending, reducing, or suppressing recombination in these structures. However, if free surfaces are defined in a more symmetric fashion, as it is possible in ultrathin released NMs, typical surface effects such as depletion, charge accumulation, or inversion[34] can be used to tailor optoelectronic properties of interest.

In this paper, we shed some light on the optical properties of transferred NMs in relation to the optical and structural properties of the system. Two transfer methods were employed and are compared through an X-ray diffraction (XRD) study that allows us to discuss the structural differences between original (before transfer) and final (after transfer) NMs containing InAs quantum dots. A photoluminescence (PL) study of released and transferred NMs is performed to relate the optical properties with our XRD results. We find that, as expected from previous studies, the release of the original layer results in a relaxed, but high quality, single crystalline NM. It is also expected that the strain release results on a red shift of the observed PL signal of the QDs. Nevertheless, we surprisingly observe a large amplification of the PL intensity for higher energies, which is more pronounced for thinner membranes. This effect is ascribed to the appearance of symmetric carrier depletion regions, consisting in a new variable for band engineering that remains poorly explored for nm-thin semiconductor systems.

Two thin film structures with nominal thicknesses of 70 and 26 nm, respectively, were grown by Molecular Beam Epitaxy (MBE) on GaAs (001) substrates using an Omicron III−V system (IFW Dresden). The structures are composed of a GaAs matrix with $Al_{0.3}Ga_{0.7}As$ barriers containing InAs QDs (1.8 ML). The growth conditions used here lead to the formation of QDs with a density of 2×10^{10} cm^{-2} and an average dot size of 20 nm diameter and 2 nm height. The MBE has a known background p-doping of $N_a = 1 \times 10^{16}$ cm^{-3}. The sample layout and a sketch of the expected confining potential are shown in Figure 1a. Before the deposition of the active layer stack, a 50 nm thick sacrificial AlAs layer was grown, which can be removed by diluted HF.[35]

In order to produce very thin NMs, two distinct release procedures were applied: the first processing method, capable of producing large area membranes, consists of defining small

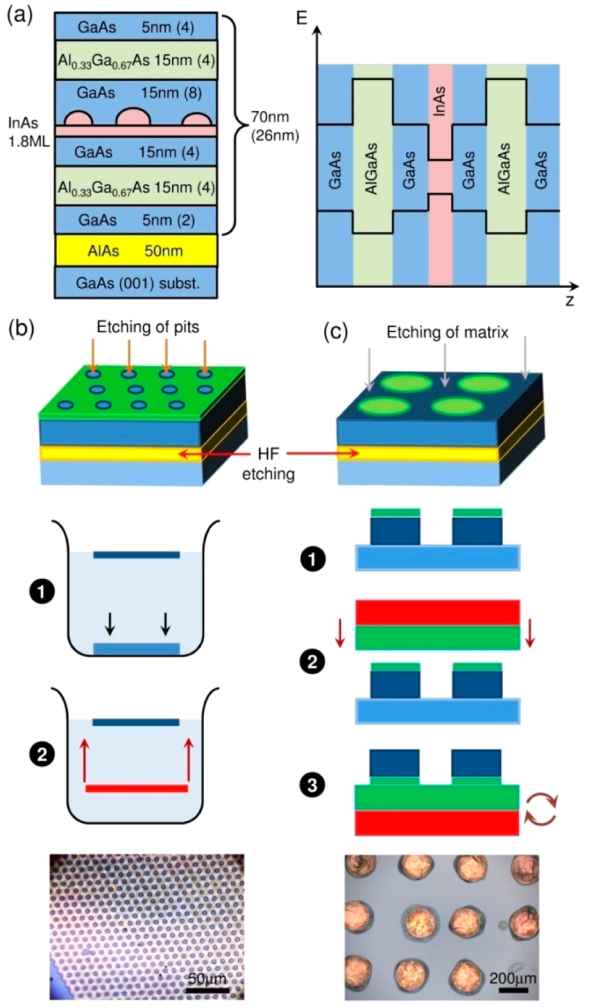

Figure 1. (a) Representation of the layer stacking in the heterostructures studied here (left panel) and sketch of their band structure (right panel). (b) Method for releasing thin membranes by lifting layers in liquid and optical image of a resulting lifted NM (lower panel).[19,36] The original substrates are represented in blue, while the new host substrates are shown in red. (c) Method for releasing thin membranes by PMMA pressing and optical image of resulting NMs.[1,22]

periodic vertical pits with a HBr (50 vol %)/$K_2Cr_2O_7$ (0.5 mol/L)/CH_3COOH (100 vol %) solution (2:1:1), so that the sacrificial layer can be accessed by an etching solution. Subsequently, by AlAs removal using diluted HF (50 vol %)/H_2O (1:800), the NM containing the topmost films is released (step 1) and lifted onto another host substrate (step 2), as depicted in Figure 1b (see refs 19 and 36 for details).

The second method of choice, more suitable for integration with flexible electronic devices, consists in defining discs with 200 μm diameter, as shown in Figure 1c. After vertical etching of the matrix (step 1) and removal of the AlAs layer, the discs are then pressed against freshly deposited polymer films (in our case PMMA, step 2), which is on the top of the new host substrate (step 3).[1,22] The final state of released NMs is shown in optical microscopy images at the bottom of Figure 1b,c. All released NMs in this work were transferred to flat epi-ready GaAs (001) substrates.

Grazing-incidence X-ray diffraction (GID) measurements near the (220) GaAs reflection were carried out at the XRD2

dx.doi.org/10.1021/ph500144s | ACS Photonics 2014, 1, 863−870

beamline of the Brazilian Synchrotron Light Laboratory (LNLS), at a fixed energy of 9 keV, 0.3° incident angle, and using a Pilatus 100 K detector integrating a 2° exit angle.[37] Low temperature photoluminescence data was acquired pumping the samples with an Ar^+ laser (λ = 514 nm). The spectrometer system (Andor Shamrock 303i) uses an Andor Si CCD with the samples installed on an open cycle He cryostat cooled down to 20 K.

In order to evaluate the crystalline quality and strain-induced modifications on the heterostructure illustrated in Figure 1a after transfer, GID reciprocal space mapping was carried out near the GaAs (220) reflection. In Figure 2a,b we show

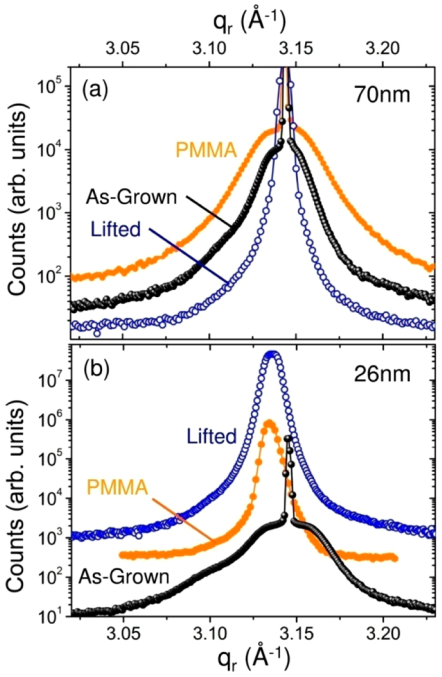

Figure 2. Grazing-incidence diffraction data measured in the vicinity of the (220) GaAs reflection for the samples studied in this work. (a) Longitudinal scans for the as-grown, lifted, and PMMA 70 nm heterostructures. (b) Longitudinal scans for all the 26 nm thick heterostructures.

longitudinal (θ-2θ) scans obtained from the 70 and 26 nm NMs, respectively. Measurements were deducted on the as-grown sample as well as on the NMs released and transferred to a new substrate by the two described methods. The original as-grown GID profiles exhibit a sharp intense peak at q_r = 3.14 Å^{-1} due to the diffraction from the GaAs (and AlGaAs) matrix. Besides this peak, a broad diffuse scattering is observed due to the InAs compressively strained QDs and regions where GaAs has tensile strain (near QD base and apex), smaller q_r values, and compressive strain (GaAs surrounding QD base), larger q_r values.[38]

The GaAs diffraction is still observed at the same position and the diffuse scattering remains mostly unchanged for curves obtained from the 70 nm thick, transferred NMs (Figure 2a). While for the PMMA sample the crystalline alignment among the membranes is preserved, the lifted NM has some foldings and therefore presents a small angular misorientation of different adjacent regions.[19] This misorientation induces a broadening of the intensity diffracted by the QDs along the reciprocal space transversal direction (q_a direction in Figure 3). Since the scattering volume must be preserved for a fixed

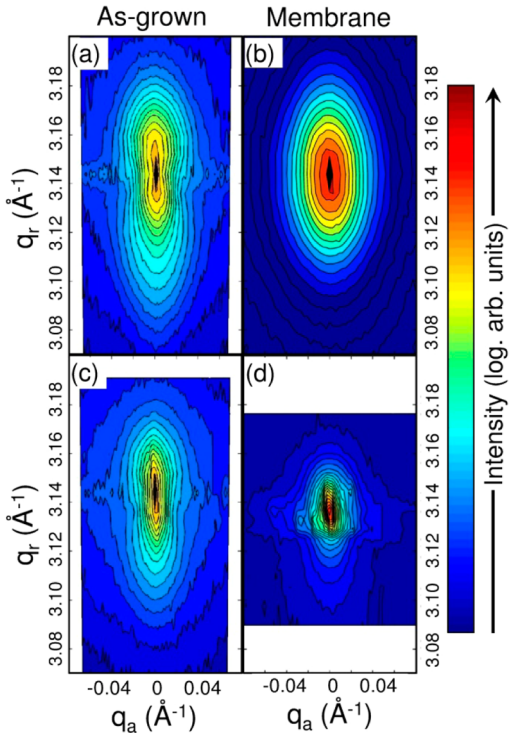

Figure 3. Complete GID maps for the as-grown and PMMA 70 nm sample are shown in (a) and (b). Reciprocal space maps for the as-grown (c) and PMMA (d) 26 nm thick heterostructures. The q_r and q_a scales are identical in all maps (white regions were not measured).

photon flux, a reduction of the amount of counts in the diffuse scattering region at the longitudinal direction is observed in the blue diffraction curve (open dots) of Figure 2a. For the 26 nm NMs, the layers are thin enough to present a modified strain status after the membrane release (compare the as-grown with the lifted and PMMA curves in Figure 2b). In such case, the sharp GaAs peak smears out due to the propagation of a modified strain field through the NMs and the overall GaAs scattering shifts toward larger lattice parameter values, reaching q_r = 3.133 Å^{-1} (a = 5.673 Å). The center of mass of the diffuse scattering is also modified. The resulting profile shown for the PMMA (orange curve in Figure 2b) and lifted NMs (blue curve in Figure 2b) points out to a lateral relaxation of the InAs lattice parameter. Additionally, one observes the appearance of a larger volume of tensile strained GaAs/AlGaAs.

For both sample structures, complete reciprocal space maps for as-grown as well as PMMA transferred NMs are depicted in Figure 3a,b for the 70 nm heterostructures and Figure 3c,d for the 26 nm heterostructures. In the two as-grown samples (Figure 3a,c), the GID maps exhibit a sharp GaAs/AlGaAs peak in both longitudinal and angular directions. After releasing, one sees that the GaAs peak position for the 70 nm NM remains almost in the same position but presents an additional broadening in the angular direction due to the appearance of a reduced misorientation (Figure 3b). The effect observed in the GID map of Figure 3d, for the thinner membrane, is again more pronounced and clearly differs from the scattering of the as-grown heterostructure (Figure 3c) along the q_r direction. The GaAs peak broadens and moves toward lower q_r, showing that the NM volume is small enough to render it much more compliant, accepting a considerable deformation due to the relaxation of the QDs.[39] The diffuse scattering also moves

dx.doi.org/10.1021/ph500144s | ACS Photonics 2014, 1, 863−870

toward lower q_v, pointing out to a lattice parameter which is, in average, larger inside the QDs. Hence, both QDs and the GaAs matrix surrounding them become structures with smoother lattice parameter gradients. Finally, we would like to mention that the GID results for reciprocal space maps in the lifted NMs are similar to these presented for the PMMA samples. However, the existence of large (mm-sized) flat areas which are slightly misoriented with respect to each other due to local folding in the NM generate more peaks along the transversal (q_a) direction of the maps, interfering with a direct interpretation of the measured signal.

Before starting a quantitative analysis of the NM systems, it should be mentioned that semiconductor nanowires (NWs) also present surface carrier trapping effects. These structures are known for having a large surface/volume ratio, and charge trapping at the surface is a key ingredient for the determination of the electronic structure of NWs even for diameters of the order of 200 nm. In these systems, depletion regions and, consequently, band bending due to charge accumulation at the surface were observed and are determinant to modify the charge distribution along the radial direction, making some radiative recombinations more or less pronounced.[40] Depletion is also a crucial parameter to explain the overall NW emission as a function of the NW radius.[41,42] It has been shown recently that photoconductivity dynamics is also modified upon charge redistribution.[43] Also for NWs, the growth of a radial heterostructure with barriers can be carried out to improve confinement and consequently light emission.[44]

To understand the observed features of the PL emission, one should first consider that in our samples the QDs are close to the surface. The pinning of the Fermi level (E_f) at the surface[45] leads to a band bending in the vicinity of this region. For GaAs (001) the Fermi level is pinned around midgap at the surface for midlevel p-doped samples, like the ones used here (see ref 46). In our case, $e{\cdot}V_s \sim 0.6$ eV, where e is the electron charge and V_s is the surface potential. Figure 4a,b shows schematically the band structure of the as-grown 70 and 26 nm samples, respectively. In these figures the width of the QD potential well was exaggerated along the growth direction for better visualization. According to Lüth,[34] the depth of the depletion region on a doped sample surface is given by $d = [V_s\varepsilon\varepsilon_0/eN_a]^{1/2}$, where ε_0 and ε are the vacuum and relative medium permittivity and N_a is the density of charge carriers at the bulk. Using the values discussed in the precedent paragraphs, we have obtained $d \sim 150$ nm. This number indicates that our QDs are inside the depletion region in both samples. In order to calculate the band bending induced by the carrier depletion one needs to calculate the Debye length, given by

$$L = \sqrt{\frac{kT\varepsilon\varepsilon_0}{2e^2N_a}}, \quad (1)$$

where k is the Boltzmann constant and $T = 20$ K. Finally, the depth (z) dependence of the potential can be expressed as

$$eV(z) = eV_s \exp(-z/L) \quad (2)$$

The resulting curvatures, similar at the near-surface region for both NM thicknesses, are directly shown in Figure 4a,b.

The energy levels of the QDs must also be calculated if one wishes to find out whether changes in the band profile lead to a repositioning of the Fermi level in which filled states can be found. Table 1 shows the calculated energies for an average InAs QD with the dimensions observed in our samples (see ref 47 for details). The calculation was carried out for a 70 nm nondepleted heterostructure band profile such as that shown in Figure 1a. Since the depletion at the QD position in Figure 4a is extremely small, these values are directly compared in Table 1 to experimentally observed transition energies, extracted from the position of InAs PL humps at the as-grown 70 nm sample (Figure 4c). In this table it is possible to see that QD heavy-hole (hh) levels are spaced by approximately 30 meV. The PL peaks that form the QD ensemble emission in Figure 4c can then be explained as being due to transitions from the fundamental electron energy level to several heavy-hole (hh) levels.[47−49] These transitions are allowed since the quantum dots do not have cylindrical symmetry. For the as-grown samples one observes that, due to the depletion, the Fermi level is positioned at ~35 meV above the bottom of the valence band at the QD position, which represents 10% of the potential well height at the valence band.

For the doping level used here the Fermi level energy is positioned within the QDs potential well, which leads to the existence of empty hh states. Figure 4c shows the PL spectra of the as-grown 70 and 26 nm samples. In both spectra the emission of the QD ensemble is observed between 1.1 and 1.4

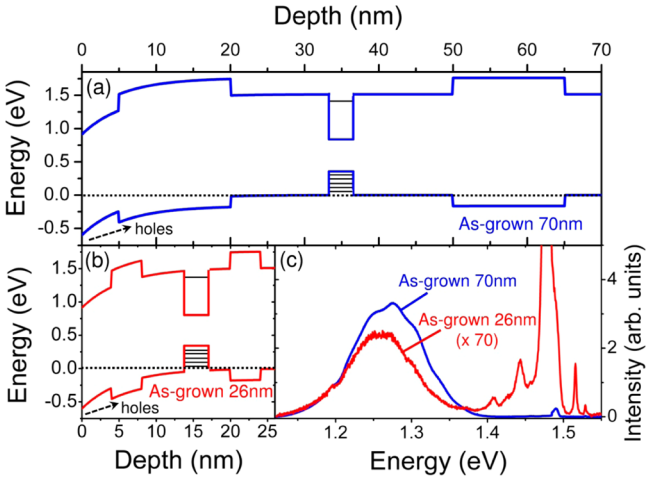

Figure 4. Sketch of the band structure of the 70 nm (a) and 26 nm (b) as-grown heterostructures. The band bending near the surface (at depth 0) is calculated using eq 2. In both diagrams the dotted line is the Fermi level. The dimension of the QD potential well is exaggerated along the growth direction for better visualization. Transition energy calculations for the QDs show the existence of a single electron level but several heavy-hole levels inside the QD potential wells. (c) PL measurements at 20 K for both as-grown heterostructures, showing a reduced emission at the 26 nm heterostructure with respect to its thicker counterpart.

Table 1. Transition Energies between the Electron Fundamental Level and Heavy Hole (hh) Levels Observed Experimentally (As-Grown 70 nm Sample) and Calculated for the QDs

transitions	experimental (eV)	calculated (eV)
*e*lhh1	1.184	1.184
*e*lhh2	1.212	1.213
*e*lhh3	1.245	1.244
*e*lhh4	1.275	1.274
*e*lhh5	1.304	1.306
*e*lhh6	1.335	1.335
*e*lhh7	1.365	1.361

dx.doi.org/10.1021/ph500144s | ACS Photonics 2014, 1, 863−870

eV. Transitions to hh excited states are denoted by the humps in this part of the spectra. One observes the recombination of seven hh excited states for the as-grown 70 nm sample, while five levels are observed for the as-grown 26 nm heterostructure. It is also clear that the emission of the QD ensemble at the 26 nm sample is much weaker than at the 70 nm. This is due to the location of the QDs inside the depletion region, which displaces holes toward deeper regions of the sample, following the electric field created by carrier depletion. The final QD emission, already excluding differences due to possible internal reflections, changes in scattering section, and efficiency of light extraction, is 2 orders of magnitude higher in the 70 nm as-grown sample than in the 26 nm as-grown sample. Another consequence of the carrier depletion observed for the 26 nm as-grown sample is the appearance of strong peaks near the GaAs gap energy. The band to band, exciton, and donor-to-carbon acceptor recombination peaks are observed at 1.519, 1.515, and 1.48 eV, respectively, while the wetting layer (WL) peak is found at 1.44 eV.

Once the PL results on the as-grown samples are understood, we can proceed to the investigation of possible modifications that take place once a NM is created. Figure 5a shows a comparison between the lifted 70 nm NM and the as-grown 70 nm sample. One observes that the QD emission increases by a factor of 2.5 for the NM in comparison to the as-grown structure. In this case, the material absence in the region of the lithographic pits makes the total area of the membrane smaller than the area with QDs for the as-grown sample. An even more pronounced result is observed for the 26 nm NM, shown in Figure 5b. The emission for the QD region of the spectra is 2 orders of magnitude larger in the NM. The enhancement factors depicted here are in agreement with relative intensities of GaAs recombination peaks, as well as the WL emission. As-grown and lifted samples were also measured in different PL setups, with distinct optical alignment and different optical paths, showing similar emission enhancement and ruling out illumination, extraction, and detection efficiency effects. Internal reflections were also ruled out by changing the incident/extraction angle with respect to the excitation laser beam. One also notices in the spectra of Figure 5b that more excited states are filled, leading to an overall enhancement of light emission at higher energies. This indicates that the PL changes from as-grown to lifted heterostructures should be attributed to the formation of new depletion regions in the NMs, which play a major role on the emission of NM systems.

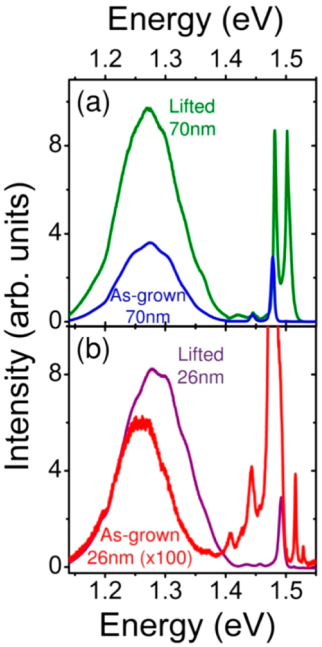

Figure 5. PL spectra before and after the releasing of NMs for the (a) 70 nm heterostructure and (b) 26 nm heterostructure. While an enhancement of the QD emission of 2.5× is observed for the thicker membrane, an enhancement factor of about 100 is obtained for the thinner membrane.

Figure 6a,b depicts the band bending obtained due to carrier depletion at the NM surfaces. In these graphical representations, the electric potentials obtained due to depletion effects at each surface are superimposed, giving rise to a symmetrically curved band profile. The electric field created at the near-surface regions drives the holes toward the central portions of the NM, improving the recombination of QD hh excited states. This effect is clearly observed here since the QD position (along the growth direction) is nearly symmetric with respect to the NM thickness. For the 70 nm NM, the strong band bending curvature at the near-surface does not impose a considerable change in the valence band energy at the QD position. A different scenario is observed for the depletion at the 26 nm membrane. For this thickness, there is a strong influence for the QDs from the electric field created on each surface. The bottom of the valence band at the QD position is now below the Fermi energy by approximately 150 meV (one-third of the quantum dot potential well height). The energy levels above the Fermi level are vacant and recombination processes can take place. However, the influx of photo-

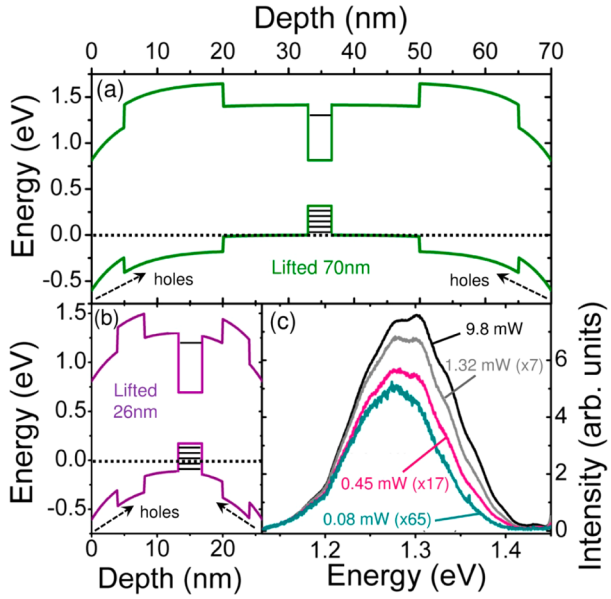

Figure 6. Representation of the band structure calculated with eq 2 for the 70 nm (a) and 26 nm (b) lifted heterostructures. The symmetric band bending on both surfaces is responsible for keeping holes inside the QDs potential well in the valence band. Transition energy calculations for the QDs show the existence of a single electron level but several heavy-hole levels inside the QD potential wells. (c) PL spectra at the QDs emission at the 26 nm lifted heterostructure region for different laser excitation powers. The depletion at the NM surfaces leads to a filling of excited states, keeping the emission at high energies even when low laser power is used.

dx.doi.org/10.1021/ph500144s | ACS Photonics 2014, 1, 863−870

generated holes populates states below the Fermi level, bringing it down and promoting a more effective recombination at higher energies. Such effect is experimentally probed by modifying the laser power, as shown in Figure 6c. Even for very small pumping power one still observes all recombination energies. If a similar measurement is carried out for the QDs sitting on a flat potential profile, excited states would no longer be visible at low pumping, leaving only the fundamental level transition signature peak.[49] When analyzing the PL enhancement in the nanomembranes, one should keep in mind that the AlGaAs barriers localize the photogenerated carriers in a region close to the quantum dots and also that the intrinsic electric field created by the surface depletion layers is relatively weak close to the QDs. The photogenerated holes are driven to the QDs, completely filling the seven hole levels and creating an attractive potential for the photogenerated electrons. Therefore, the single QD electron level is kept occupied even at low excitation powers. Similar measurements were also performed on the PMMA NMs. However, for these samples, the polymer luminescence is too intense to allow the observation of a clear and isolated membrane signal. In ref 22, a much thicker NM (200−250 nm) is placed on top of PMMA, reducing the polymer emission.

Finally, in Figure 5, red shifts of the order of 5 meV are observed for the localized humps in the QD ensemble emission after the NM release. This is consistent with the lattice relaxation in the quantum dots inferred from the X-ray scattering data shown in Figure 2 and comparable with the shifts observed in III−V NMs in ref 20. Nevertheless, 5 meV is a small value compared to the major changes produced by the charge depletion originated from the NM lifting, as explained in this work, making the resulting depletion effect much more relevant for band engineering.

In conclusion, we transferred two heterostructures containing QDs, using different techniques, to a new host substrate. A rigorous structural characterization using GID was carried out to investigate the strain state as well as the crystal quality of the transferred structures. Furthermore, PL investigation of the same samples allows for the determination of the optical properties. Our GID results confirm the previously reported high crystal quality of the transferred NMs. We observe a complete strain relaxation of our NMs after transfer, influencing the investigated optical properties of the structures. Surprisingly, a large enhancement of the PL peak intensity of our QD samples for the 26 nm thick NM is observed. We ascribe this effect to the formation of symmetrically located depletion areas near to the sample surface, which lead to an accumulation of holes near the QD. The band bending was calculated and points out to a scenario which is in agreement with experimental results. Therefore, this effect is solely arising from the reduced thickness and not a previously observed interference effect.[20] In a more general frame, depletion can also be used to increase or reduce the concentration of carriers in specific regions of NMs, since it can be tuned by changing the doping (N_a in eq 1), the type of semiconductor (ε in eq 1, V_s in eq 2) and the position of the active layer inside the NM (symmetric or asymmetric position). Dynamic carrier trap filling under periodic light pumping conditions was also observed for NWs exhibiting surface carrier depletion (see ref 43) and can be used to tune time-dependent behavior in NM systems. Finally, our detailed investigations allow a better understanding of this kind of NM transferred systems. Such systems have been used to tune the emission of single QDs into resonance, whereby the ability to strain such membranes was the major tuning knob.[21] The mechanical flexibly of the NM increases linearly with the reduction of the thickness for these membranes[1] making ultrathin membranes in the range below 30 nm the most interesting structures for strain transfer by embedded nanostructures.[39] Very thin NMs are also mandatory for applications demanding extremely high curvatures or high strain transfer to the membrane. For such systems the usual tuning mechanisms of semiconductor heterostructure design such as quantum well thickness and barrier thickness cannot be freely used as this may render the structure too thick. Therefore, an additional tuning mechanism is needed to specify the optical properties of the NM. The observed shift and enhancement of the optical InAs QD signal by surface depletion effects associated with the amount of free carriers inside the structure (doping) offers one of these needed tuning knobs for NMs. Doping is a highly controlled process in semiconductor growth and does not influence the overall thickness of the heterostructures. It allows, therefore, tuning and enhancing of the optical properties for such ultrathin NMs.

AUTHOR INFORMATION

Corresponding Author

*E-mail: angelomalachias@gmail.com.

Notes

The authors declare no competing financial interest.

ACKNOWLEDGMENTS

The authors acknowledge FAPEMIG, FAPESP (CD: Project 2011/22945−1), CAPES, and CNPq for financial support. We thank Maria Helena de Oliveira Piazzeta (LNNano Microfabrication laboratory) for her support on lithographic processing. Beamtime was granted on the XRD2 beamline by the LNLS/MCTI.

REFERENCES

(1) Rogers, J. A.; Lagally, M. G.; Nuzzo, R. G. Synthesis, assembly and applications of semiconductor nanomembranes. *Nature* **2011**, *477* (7362), 45−53.

(2) Rogers, J. A. Slice and dice, peel and stick: Emerging methods for nanostructure fabrication. *ACS Nano* **2007**, *1*, 151−153.

(3) Scott, S. A.; Peng, W. N.; Kiefer, A. M.; Jiang, H. Q.; Knezevic, I.; Savage, D. E.; Eriksson, M. A.; Lagally, M. G. Influence of surface chemical modification on charge transport properties in ultrathin silicon membranes. *ACS Nano* **2009**, *3*, 1683−1692.

(4) Chen, F.; Ramayya, E. B.; Euaruksakul, C.; Himpsel, F. J.; Celler, G. K.; Ding, B. J.; Knezevic, I.; Lagally, M. G. Quantum confinement, surface roughness, and the conduction band structure of ultrathin silicon membranes. *ACS Nano* **2010**, *4*, 2466−2474.

(5) Kiefer, A. M.; Paskiewicz, D. M.; Clausen, A. M.; Buchwald, W. R.; Soref, R. A.; Lagally, M. G. Si/Ge junctions formed by nanomembrane bonding. *ACS Nano* **2011**, *5*, 1179−1189.

(6) Yu, M. R.; Huang, Y.; Ballweg, J.; Shin, H.; Huang, M. H.; Savage, D. E.; Lagally, M. G.; Dent, E. W.; Blick, R. H.; Williams, J. C. Semiconductor nanomembrane tubes: Three-dimensional confinement for controlled neurite outgrowth. *ACS Nano* **2011**, *5*, 2447−2457.

(7) Paskiewicz, D. M.; Tanto, B.; Savage, D. E.; Lagally, M. G. Defect-free single-crystal SiGe: A new material from nanomembrane strain engineering. *ACS Nano* **2011**, *5*, 5814−5822.

(8) Paskiewicz, D. M.; Scott, S. A.; Savage, D. E.; Celler, G. K.; Lagally, M. G. Symmetry in strain engineering of nanomembranes: Making new strained materials. *ACS Nano* **2011**, *5*, 5532−5542.

(9) Cavallo, F.; Grierson, D. S.; Turner, K. T.; Lagally, M. G. "Soft Si": Effective stiffness of supported crystalline nanomembranes. *ACS Nano* **2011**, *5*, 5400−5407.
(10) Sookchoo, P.; Sudradjat, F. F.; Kiefer, A. M.; Durmaz, H.; Paiella, R.; Lagally, M. G. Strain engineered SiGe multiple-quantum-well nanomembranes for far-infrared intersubband device applications. *ACS Nano* **2013**, *7*, 2326−2334.
(11) Zaumseil, J.; Meitl, M. A.; Hsu, J. W. P.; Acharya, B. R.; Baldwin, K. W.; Loo, Y.-L.; Rogers, J. A. Three-dimensional and multilayer nanostructures formed by nanotransfer printing. *Nano Lett.* **2003**, *3*, 1223−1227.
(12) Kim, D.-H.; Viventi, J.; Amsden, J. J.; Xiao, J.; Vigeland, L.; Kim, Y.-S.; Blanco, J. A.; Panilaitis, B.; Frechette, E. S.; Contreras, D.; Kaplan, D. L.; Omenetto, F. G.; Huang, Y.; Hwang, K.-C.; Zakin, M. R.; Litt, B.; Rogers, J. A. Dissolvable films of silk fibroin for ultrathin conformal biointegrated electronics. *Nat. Mater.* **2010**, *9*, 511−517.
(13) Choi, W. M.; Song, J.; Khang, D.-Y.; Jiang, H.; Huang, Y. Y.; Rogers, J. A. Biaxially stretchable "wavy" silicon nanomembranes. *Nano Lett.* **2007**, *7*, 1655−1663.
(14) Chen, L.; Yang, H.; Qiang, Z.; Pang, H.; Sun, L.; Ma, Z.; Pate, R.; Roberts, A. S.; Gao, S.; Xu, J.; Brown, G. J.; Zhou, W. Colloidal quantum dot absorption enhancement in flexible Fano filters. *Appl. Phys. Lett.* **2010**, *96*, 083111.
(15) Zhang, Y.; Yu, M.; Savage, D. E.; Lagally, M. G.; Blick, R. H.; Liu, F. Effect of surface bonding on semiconductor nanoribbon wiggling structure. *Appl. Phys. Lett.* **2010**, *96*, 111904.
(16) Kim, D.-H.; Rogers, J. A. Bend, buckle, and fold: Mechanical engineering with nanomembranes. *ACS Nano* **2009**, *3*, 498−501.
(17) Chanda, D.; Shigeta, K.; Gupta, S.; Cain, T.; Carlson, A.; Mihi, A.; Baca, A. J.; Bogart, G. R.; Braun, P.; Rogers, J. A. Large-area flexible 3D optical negative index metamaterial formed by nanotransfer printing. *Nat. Nanotechnol.* **2011**, *6*, 402−207.
(18) Hwang, S.-W.; Tao, H.; Kim, D.-H.; Cheng, H.; Song, J.-K.; Rill, E.; Brenckle, M. A.; Panilaitis, B.; Won, S. M.; Kim, Y.-S.; Song, Y. M.; Yu, K. J.; Ameen, A.; Li, R.; Su, Y.; Yang, M.; Kaplan, D. L.; Zakin, M. R.; Slepian, M. J.; Huang, Y.; Omenetto, F. G.; Rogers, J. A. A physically transient form of silicon electronics. *Science* **2012**, *337*, 1640−1644.
(19) Malachias, A.; Mei, Y.; Annabattula, R. K.; Deneke, Ch.; Onck, P. R.; Schmidt, O. G. Wrinkled-up nanochannel networks: Long-range ordering, scalability, and X-ray investigation. *ACS Nano* **2008**, *2*, 1715−1721.
(20) Mei, Y.; Kiravittaya, S.; Benyoucef, M.; Thurmer, D. J.; Zander, T.; Deneke, Ch.; Cavallo, F.; Rastelli, A.; Schmidt, O. G. Optical properties of a wrinkled nanomembrane with embedded quantum well. *Nano Lett.* **2007**, *7*, 1676−1679.
(21) Rastelli, A.; Ding, F.; Plumhof, J. D.; Kumar, S.; Trotta, R.; Deneke, C.; Malachias, A.; Atkinson, P.; Zallo, E.; Zander, T.; et al. Controlling quantum dot emission by integration of semiconductor nanomembranes onto piezoelectric actuators. *Phys. Status Solidi B* **2012**, *249*, 687−696.
(22) Ding, F.; Singh, R.; Plumhof, J. D.; Zander, T.; Krapek, V.; Chen, Y. H.; Benyoucef, M.; Zwiller, V.; Dorr, K.; Bester, G.; Rastelli, A.; Schmidt, O. G. Tuning the exciton binding energies in single self-assembled InGaAs/GaAs quantum dots by piezoelectric-induced biaxial stress. *Phys. Rev. Lett.* **2010**, *104*, 067405.
(23) Deneke, C.; Malachias, A.; Kiravittaya, S.; Benyoucef, M.; Metzger, T. H.; Schmidt, O. G. Strain states in a quantum well embedded into a rolled-up microtube: X-ray and photoluminescene studies. *Appl. Phys. Lett.* **2010**, *96*, 143101.
(24) Kipp, T.; Strelow, C.; Welsch, H.; Heyn, C.; Heitmann, D. Optical microtube ring resonators. *Phys. Semicond., Parts A and B* **2007**, *893*, 1127−1128.
(25) Jons, K. D.; Hafenbrak, R.; Singh, R.; Ding, F.; Plumhof, J. D.; Rastelli, A.; Schmidt, O. G.; Bester, G.; Michler, P. Dependence of the redshifted and blueshifted photoluminescence spectra of single InGaAs/GaAs quantum dots on the applied uniaxial stress. *Phys. Rev. Lett.* **2011**, *107*, 217402.
(26) Zhen, H. L.; Huang, G. S.; Kiravittaya, S.; Li, S. L.; Deneke, Ch.; Thurmer, D. J.; Mei, Y. F.; Schmidt, O. G.; Lu, W. Light-emitting properties of a strain-tuned microtube containing coupled quantum wells. *Appl. Phys. Lett.* **2013**, *102*, 041109.
(27) Hosoda, M.; Kishimoto, Y.; Sato, M.; Nashima, S.; Kubota, K.; Saravanan, S.; Vaccaro, P. O.; Aida, T.; Ohtani, N. Quantum-well microtube constructed from a freestanding thin quantum-well layer. *Appl. Phys. Lett.* **2003**, *83*, 1017.
(28) Kubota, K.; Vaccaro, P. O.; Ohtani, N.; Hirose, Y.; Hosoda, M.; Aida, T. Photoluminescence of GaAs/AlGaAs micro-tubes containing uniaxially strained quantum wells. *Physica E* **2002**, *13*, 313−316.
(29) Ohtani, N.; Kishimoto, K.; Kubota, K.; Saravanan, S.; Sato, Y.; Nashima, S.; Vaccaro, P.; Aida, T.; Hosoda, M. Uniaxial-strain-induced transition from type-II to type-I band configuration of quantum well microtubes. *Physica E* **2004**, *21*, 732−736.
(30) Kipp, T.; Welsch, H.; Strelow, Ch.; Heyn, Ch.; Heitmann, D. Optical modes in semiconductor microtube ring resonators. *Phys. Rev. Lett.* **2006**, *96*, 077403.
(31) Li, F.; Mi, Z.; Vicknesh, S. Coherent emission from ultrathin-walled spiral InGaAs/GaAs quantum dot microtubes. *Opt. Lett.* **2009**, *34* (No. 19), 2915−2917.
(32) Bianucci, P.; Mukherjee, S.; Dastjerdi, M. H. T.; Poole, P. J.; Mi, Z. Self-organized InAs/InGaAsP quantum dot tube lasers. *Appl. Phys. Lett.* **2012**, *101*, 031104.
(33) Bimberg, D.; Grundmann, M.; Ledentsov, N. N. *Quantum Dot Heterostructures*; Wiley: New York, 1999.
(34) Lüth, H. *Solid Surfaces, Interfaces and Thin Films*; Springer: Berlin, 2001.
(35) Yablonovitch, E.; Gmitter, T.; Harbison, J. P.; Bhat, R. Extreme selectivity in the lift-off of epitaxial GaAs films. *Appl. Phys. Lett.* **1987**, *51*, 2222.
(36) Roberts, M. M.; Klein, L. J.; Savage, D. E.; Slinker, K. A.; Friesen, M.; Celler, G.; Eriksson, M. A.; Lagally, M. G. Elastically relaxed free-standing strained-silicon nanomembranes. *Nat. Mater.* **2006**, *5*, 388−393.
(37) Malachias, A.; Magalhaes-Paniago, R.; Neves, B. R. A.; Rodrigues, W. N.; Moreira, M. V. B.; Pfannes, H.-D.; de Oliveira, A. G.; Kycia, S.; Metzger, T. H. Direct observation of the coexistence of coherent and incoherent InAs self-assembled dots by X-ray scattering. *Appl. Phys. Lett.* **2001**, *79*, 4342.
(38) Hesse, A.; Stangl, J.; Holy, V.; Roch, T.; Bauer, G.; Schmidt, O. G.; Denker, U.; Struth, B. Effect of overgrowth on shape, composition, and strain of SiGe islands on Si(001). *Phys. Rev. B* **2002**, *66*, 085321.
(39) Deneke, Ch.; Malachias, A.; Rastelli, A.; Merces, L.; Huang, M.; Cavallo, F.; Schmidt, O. G.; Lagally, M. G. Straining nanomembranes via highly mismatched heteroepitaxial growth: InAs islands on compliant Si substrates. *ACS Nano* **2012**, *6*, 10287−10295.
(40) Liao, Z.-M.; Zhang, H.-Z.; Zhou, Y.-B.; Xu, J.; Zhang, J.-M.; Yu, D.-P. Surface effects on photoluminescence of single ZnO nanowires. *Phys. Lett. A* **2008**, *372*, 4505−4509.
(41) Demichel, O.; Heiss, M.; Bleuse, J.; Mariette, H.; Fontcuberta, i; Morral, A. Impact of surfaces on the optical properties of GaAs nanowires. *Appl. Phys. Lett.* **2010**, *97*, 201907.
(42) Heiss, M.; Colombo, C.; Fontcuberta, i; Morral, A. Nanowire based heterostructures: Fundamental properties and applications. *Proc. SPIE* **2011**, *8106*, 810603.
(43) Beaudoin, A.; Salem, B.; Baron, T.; Gentile, P.; Morris, D. Impact of n-type doping on the carrier dynamics of silicon nanowires studied using optical-pump terahertz-probe spectroscopy. *Phys. Rev. B* **2014**, *89*, 115316.
(44) Fontcuberta, i; Morral, A.; Spirkoska, D.; Arbiol, J.; Heigoldt, M.; Morante, J. R.; Abstreiter, G. Prismatic quantum heterostructures synthesized on molecular-beam epitaxy GaAs nanowires. *Small* **2008**, *4*, 899−903.
(45) Spicer, W. E.; Chye, P. W.; Skeath, P. R.; Su, C. Y.; Lindau, I. New and unified model for Schottky barrier and III−V insulator interface states formation. *J. Vac. Sci. Technol.* **1979**, *16*, 1422.

(46) Pashley, M. D.; Haberern, K. W.; Feenstra, R. M.; Kirchner, P. D. Different Fermi-level pinning behavior on n- and p-type GaAs(001). *Phys. Rev. B* **1993**, *48*, 4612−4615.
(47) Safar, G. A. M.; Rodrigues, W. N.; Cury, L. A.; Chacham, H.; Moreira, M. V. B.; Freire, S. L. S.; deOliveira, A. G. Effect of Te as a surfactant on the optical properties of InAs self-assembled quantum dots. *Appl. Phys. Lett.* **1997**, *71* (4), 521−523.
(48) Kiravittaya, S.; Rastelli, A.; Schmidt, O. G. Photoluminescence from seeded three-dimensional InAs/GaAs quantum-dot crystals. *Appl. Phys. Lett.* **2006**, *88*, 043112.
(49) Grundmann, M.; Ledentsov, N. N.; Stier, O.; Bimberg, D.; Ustinov, V. M.; Kopev, P. S.; Alferov, Zh. I. Excited states in self-organized InAs/GaAs quantum dots: Theory and experiment. *Appl. Phys. Lett.* **1996**, *68*, 979−981.